Singular Value Optimization for Multifrequency Multimonostatic Inverse Scattering Over Circular Domains Under the Born Approximation

Amedeo Capozzoli, Claudio Curcio, and Angelo Liseno

Abstract – We extend singular value optimization to inverse scattering under the Born approximation in a two-dimensional geometry using a multifrequency multimonostatic measurement configuration with transmitters and receivers arranged over a circular domain. We optimize the transmitter and receiver locations, as well as the frequency sampling step, and we numerically study the performance of the method for aspect-limited acquisitions.

1. Introduction

Optimal sensors placement is relevant in many disciplines, as control systems [1], fault detection [2], target location [3], and environment understanding for autonomous machine maneuvering [4]. In electromagnetics, optimizing the sensor locations arises in inverse source and inverse scattering to extract as much information as possible from the investigated scenario for the targeted purpose, given some a priori information on the scenario itself [5–7].

Inverse source requires selecting the minimum number of field sensors and locations to reconstruct the radiators with the best possible performance in terms of conditioning of the underlying linear inverse problem [6]. To this end, the singular value optimization (SVO) has been introduced [6]. It consists of optimizing the singular value (SV) behavior of the matrix discretizing the radiation problem. The approach can be regarded as a way to maximize the amount of information collected by sensors on the unknown [8], and its optimality has been shown in [9]. Moreover, SVO has undergone an extensive experimental validation [10–12] and has proven successful in determining the number of samples and the positions for the reconstruction of a source.

SVO can be applied to linear inverse scattering also [7], allowing the possibility to deal with questions of particular interest in this field. In particular, in such applications, selecting the minimum number of field sensors and locations, as well as the minimum number and locations of the illuminating sources and of the interrogating frequencies in the considered band of interest is relevant [7] to reconstruct the scenario with the best possible performance for conditioning of the underlying linear inverse problem. In [7], SVO was much more efficient than the typical uniform sampling criterion to reconstruct scatterers under the Born approximation.

We extend SVO to inverse scattering under the Born approximation in a two-dimensional (2D) geometry. In particular, in [7], the illumination was performed with a multifrequency single-view plane wave, and acquisition was carried out over a rectilinear domain. Here, we use a multifrequency multimonostatic measurement configuration with transmitters and receivers arranged over a circular domain in the near field of the scatterer. Furthermore, differently than [7], we optimize the transmitter and receiver locations, as well as the frequency sampling step, and we numerically study the performance of the method for aspect-limited acquisitions. In this article, we consider a canonical measurement configuration, although SVO is able to deal with inverse scattering problems under general acquisition geometries.

Manuscript received 27 December 2022.

Amedeo Capozzoli, Claudio Curcio, and Angelo Liseno are with the Universitá di Napoli Federico II, Dipartimento di Ingegneria Elettrica e delle Tecnologie dell'Informazione (DIETI), via Claudio 21, I 80125 Napoli, Italy; e-mail: a.capozzoli@unina.it.

2. The Inverse Scattering Problem and the Inversion Approach

Figure 1 illustrates the 2D transverse magnetic geometry of the problem along with the multimonostatic acquisition strategy: a unique transmitter and receiver moves over a measurement circle of radius r. The unknown objects are assumed in the $\mathcal{R} = [-x_M, x_M] \times [-y_M, y_M]$ box, and the embedding medium is free space having ε_0 and μ_0 as permittivity and permeability, respectively. The transmitter is a pointlike source with excitation I, while the receiver is an ideal probe sampling the scattered E-field pointwise. According to such hypotheses, the problem is scalar and the only (z) component of the scattered field, apart from normalization to $-j\beta^2/4$, is

$$E_s(\theta_i, \beta) = \iint_{\mathcal{R}} E(x', y'; \theta_i)\chi(x', y')G(\theta_i; \beta; x', y')dx'dy', \tag{1}$$

where β is the wavenumber, the Cartesian components of the transmitter/receiver locations are $(r\cos\theta_i, r\sin\theta_i)$, $G(\theta_i; \beta; x', y') = H_0^{(2)}\left(\beta\sqrt{(r\cos\theta_i - x')^2 + (r\sin\theta_i - y')^2}\right)$, $H_0^{(2)}(\cdot)$ is the Hankel function of zeroth order and second kind, E is the total E field in $\mathcal{R}$, and $\chi(x', y') = (\varepsilon(x', y') - \varepsilon_0)/\varepsilon_0$ is the dimensionless contrast function, the unknown of the problem. In (1), we account for the aspect limitation by setting $\theta_i \in (\theta_1, \theta_2)$. Furthermore,

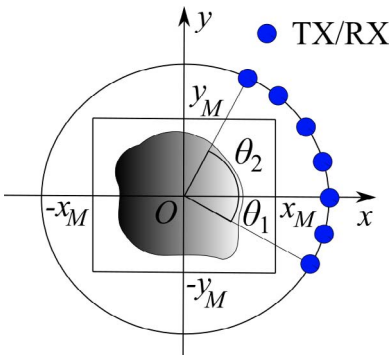

Figure 1. Multimonostatic measurement configuration.

we assume that the multifrequency data are dealt with by wavenumber $\beta \in (\beta_{\min}, \beta_{\max})$ due to features of the acquisition system, where $\beta_{\min}$ and $\beta_{\max}$ correspond to the minimum and maximum used frequencies, respectively.

Under the Born approximation, (1) becomes

$$E_s(\theta_i, \beta) = -\frac{I\beta^2}{4\omega\epsilon_0} \iint_{\mathcal{R}} \chi(x', y') G^2(\theta_i; \beta; x', y') dx' dy'. \tag{2}$$

The objects are illuminated from N, possibly unequally spaced angular locations $\{\theta_{i_n}\}_{n=1}^{N}$ at M, possibly unequally spaced wavenumbers β_m, and the scattered field is simultaneously acquired at the same locations. In principle, the angular locations θ_{i_n} should change, depending on the wavenumber. However, to make the measurement configuration practical, θ_{i_n} is unique for all frequencies, while the frequencies are equally spaced with a step Δf to be optimized. Accordingly, SVO is in charge of optimizing θ_{i_n} and Δf.

Although other choices are possible [7], we represent the problem unknown χ by a piecewise constant function so that (2) can be discretized as

$$\underline{E}_s = \underline{\underline{T}}\ \underline{\chi}. \tag{3}$$

The generic element χ_t of vector $\underline{\chi}$ contains the samples $\chi_{pq} = \chi(x'_p, y'_q)$ of the problem unknown at the points (x'_p, y'_q), with $x'_p = p\Delta x$, $y'_q = q\Delta y$, $p = -P, \ldots, P$, $q = -Q, \ldots, Q$, $2P + 1 = 2x_M/\Delta x$, and $2Q + 1 = 2y_M/\Delta y$. In (3), the index mapping $t = t(p, q)$ has been adopted. Moreover, $\underline{E}_s$ is the vector containing the $N \times M$ field samples $E_s(\theta_{i_n}, \beta_m)$, while the generic matrix entry is

$$T_{\text{st}} = \frac{j}{16} \frac{I\beta^4}{\omega\epsilon_0} \Delta x \Delta y G^2(\theta_{i_n}; \beta_m; x'_p, y'_q), \tag{4}$$

where $s = s(n, m)$.

The problem amounts to determining χ in terms of χ_{pq} from the scattered field samples. The inversion of (3) is ill conditioned, and a regularized approach should be exploited. As a possible solution, the truncated singular value decomposition [9] is adopted, even if other regularization strategies are possible [13] and have been proposed in this framework [14].

3. Choice of Number and Locations of Near-Field Samples

Matrix $\underline{\underline{T}}$ is not univocally defined because it depends on N, M, $\{\theta_{i_n}\}_{n=1}^{N}$ and Δf. A family of matrices $\underline{\underline{T}}$ is then available, with different behaviors of the SVs. Such a degree of freedom enables choosing θ_{i_n}, providing the largest possible SV (normalized to the first one) behavior, a condition reducing noise amplification effects during the inversion and increasing the collected information. This can be performed by maximizing the functional [5]

$$\Phi(N, M, \theta_{i_1}, \theta_{i_2}, \ldots, \theta_{i_N}) = \sum_{k=1}^{K} \frac{\sigma_k}{\sigma_1}, \tag{5}$$

where $K = \min\{NM,\ PQ\}$ and σ_k is the SV of $\underline{\underline{T}}$. We notice that the previously mentioned degree of freedom can be exploited along a different rationale [8, 15]. For fixed N and M, the maximization of Φ leading to the $\Phi_{\text{opt}}(N,\ M)$ value improves the information carried by the scattered field on the observation domain with just $N \times M$ probing. However, by increasing N and M, it is expected that $\Phi_{\text{opt}}(N,\ M)$ increases but not indefinitely: too many field samples and frequencies too close each other do not provide independent information [16]. Accordingly, $\Phi_{\text{opt}}(N,\ M)$ as a function of N and M must exhibit a saturation behavior. The values of N and M at the saturation knee represent the minimum number of samples needed to achieve all the information available on χ from the domain $(\theta_1,\ \theta_2) \times (\beta_{\min},\ \beta_{\max})$.

To favor a successful optimization process, the sampling locations are represented with a low number of parameters by a properly defined mapping function [8–12]. In addition, proper constraints are enforced to ensure that $\theta_{i_n} \in (\theta_1, \theta_2)$, $n = 1, \ldots, N$ [17, 18]. Also, to further simplify the determination of the optimal M avoiding a 2D search, we compute several optimizations of Φ for a fixed value of M, thus obtaining $\Phi_{\text{opt}}(N)$ curves parameterized over M. For an increasing M, such curves increase their values, and we raise M until $\Phi_{\text{opt}}(N)$ does not significantly change.

4. Numerical Results

The results refer to a 0.2 m × 0.2 m investigation domain, with a measurement circle of radius $r = 1.5x_M$ and a frequency range from 0.5 GHz to 7 GHz. The optimized measurement configuration has been used to invert numerical data generated by using the algorithm in [19] and referring to two identical cylinders having radii equal to 1 cm, relative dielectric permittivity equal to 1.5 and located at (5, 5)cm and (–5, –5)cm, respectively. The numerical data have been corrupted by noise with a signal-to-noise ratio of 40 dB, a typical

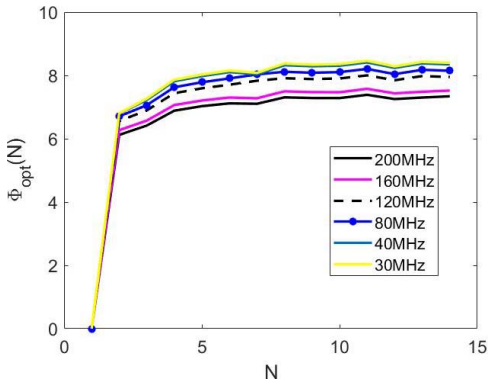

Figure 2. The $\Phi_{opt}(N)$ curves for different values of Δf.

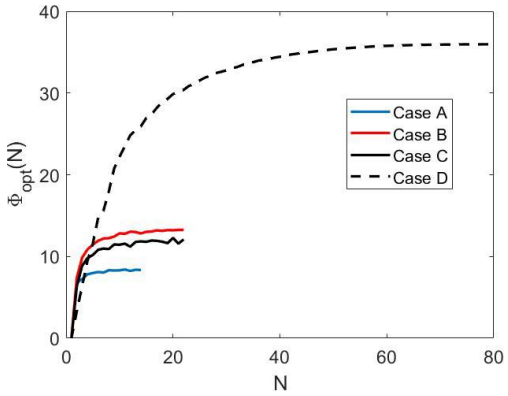

Figure 3. The $\Phi_{opt}(N)$ curves for cases A to D.

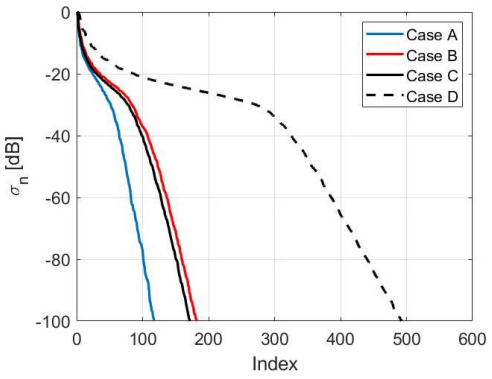

Figure 4. The SVs for cases A to D.

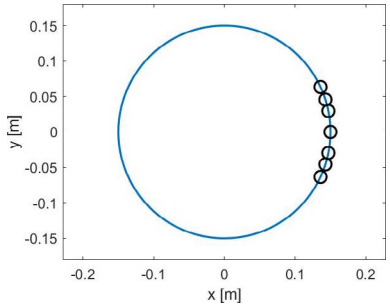

Figure 5. Sampling points for case A.

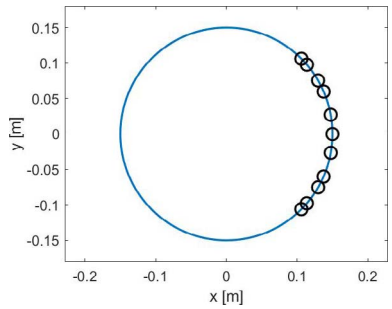

Figure 6. Sampling points for case B.

value in tomographic applications [20, 21]. The values of M and N have been chosen as those corresponding to increases of $\Phi_{opt}(N, M)$ of less than 2%.

Results for different levels of aspect limitations are provided. In particular, the cases of symmetrical domains with $\theta_2 = -\theta_1 = 25°$ (case A) and $\theta_2 = -\theta_1 = 45°$ (case B), of an asymmetrical domain with $\theta_1 = -10°$ and $\theta_2 = 80°$ (case C), and an angular complete domain with $\theta_2 = -\theta_1 = 180°$ (case D) are considered.

To choose Δf, in Figure 2, the $\Phi_{opt}(N)$ curves for different values of Δf are shown. The curves approximately saturate around $\Delta f = 40$ MHz so that such a value has been chosen as the optimal frequency sampling step.

Once Δf has been selected, the $\Phi_{opt}(N)$ curves for cases A to D are summarized in Figure 3. We deduce that the number of sampling points corresponding to the knee is $N = 7$, $N = 11$, $N = 11$, and $N = 39$ for cases A to D, respectively. The corresponding SVs are shown in Figure 4.

The optimized sampling points are reported in Figures 5–8 for cases A to D, respectively. As expected, the resulting sampling is nonuniform, except for case D, corresponding to an angular complete domain.

Finally, the reconstructions are depicted in Figures 9–12, for cases A to D, respectively. The reconstruction quality improves as long the aspect limitation of the data is reduced. The angular complete case offers also the possibility to perform quantitative reconstructions.

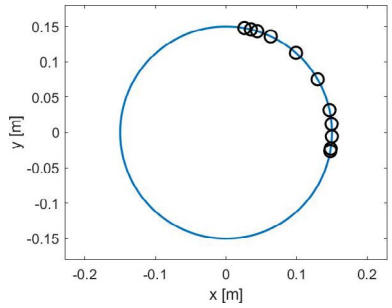

Figure 7. Sampling points for case C.

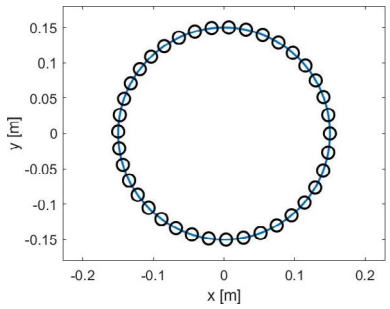

Figure 8. Sampling points for case D.

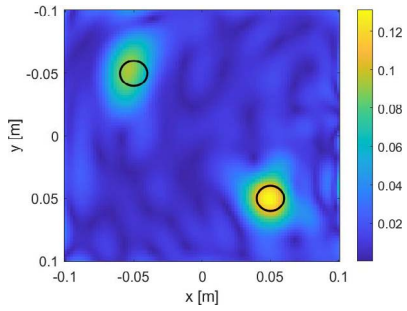

Figure 9. Contrast function reconstruction for case A.

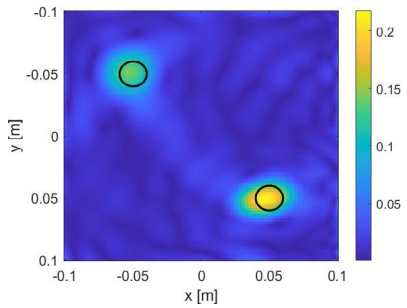

Figure 10. Contrast function reconstruction for case B.

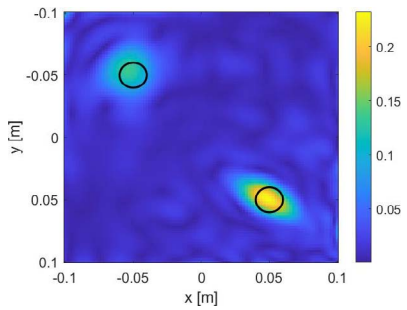

Figure 11. Contrast function reconstruction for case C.

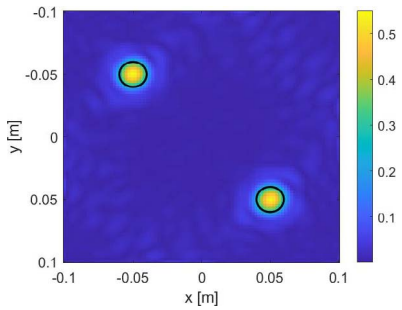

Figure 12. Contrast function reconstruction for case D.

5. Conclusions

We have applied SVO for the first time to a 2D inverse scattering problem using a multifrequency multimonostatic measurement configuration with near-field measurements, linearized under the Born approximation. The reconstruction of two dielectric cylinders with a circular cross section has been addressed. The SVO has shown to be capable to properly locate the sampling points, taking into account aspect-limited acquisitions and leading to successful reconstructions. Extensions of this work consider the application of SVO to other linearizing approximations as the distorted Born approximation [22] and to noncanonical acquisition geometries.

6. References

1. D. J. Chmielewski, T. Palmer, and V. Manousiouthakis, "On the Theory of Optimal Sensor Placement," *AIChE Journal*, **48**, 5, May 2002, pp. 1001-1012.
2. K. Worden and A. P. Burrows, "Optimal Sensor Placement for Fault Detection," *Engineering Structures*, **23**, 8, August 2001, pp. 885-901.
3. F. Y. S. Lin and P. L. Chiu, "A Near-Optimal Sensor Placement Algorithm to Achieve Complete Coverage/ Discrimination in Sensor Networks," *IEEE Communications Letters*, **9**, 1, January 2005, pp. 43-45.
4. H. Zhang, "Two-Dimensional Optimal Sensor Placement," *IEEE Transactions on Systems, Man, and Cybernetics*, **25**, 5, May 1995, pp. 781-792.
5. A. J. Devaney, *Mathematical Foundations of Imaging, Tomography and Wavefield Inversion*, New York, Cambridge University Press, 2012.
6. A. Capozzoli, C. Curcio, A. Liseno, and P. Vinetti, "Field Sampling and Field Reconstruction: A New Perspective," *Radio Science*, **45**, 6, December 2010, p. RS6004.
7. A. Capozzoli, C. Curcio, and A. Liseno, "Singular Value Optimization in Inverse Electromagnetic Scattering," *IEEE Antennas and Wireless Propagation Letters*, **16**, 2017, pp. 1094-1097.
8. A. Capozzoli, C. Curcio, and A. Liseno, "Different Metrics for Singular Value Optimization in Near-Field Antenna Characterization," *Sensors*, **21**, 6, March 2021, p. 2122.
9. A. Capozzoli, C. Curcio, and A. Liseno, "On the Optimal Field Sensing in Near-Field Characterization," *Sensors*, **21**, 13, June 2021, p. 4460.
10. A. Capozzoli, C. Curcio, and A. Liseno, "Experimental Field Reconstruction of Incoherent Sources," *Progress in*

Electromagnetics Research B, **47**, February 2013, pp. 219-239.

11. A. Capozzoli, C. Curcio, and A. Liseno, "Optimized Spherical Near-Field Antenna Measurements," The 8th European Conference on Antennas and Propagation, The Hague, The Netherlands, April 6–11, 2014, pp. 1685-1689.
12. A. Capozzoli, C. Curcio, and A. Liseno, "Optimized Near Field Antenna Measurements in the Cylindrical Geometry," 2015 9th European Conference on Antennas and Propagation, Lisbon, Portugal, April 13–17, 2015, pp. 1-5.
13. A. Kirsch, *An Introduction to the Mathematical Theory of Inverse Problems*, Bristol, NY, Springer-Verlag, 1996.
14. A. Capozzoli, C. Curcio, and A. Liseno, "Regularization of Residual Ill-Conditioning in Planar Near-Field Measurements," 2016 10th European Conference on Antennas and Propagation, Davos, Switzerland, April 10–15, 2016, pp. 1-4.
15. J. Ranieri, A. Chebira, and M. Vetterli, "Near-Optimal Sensor Placement for Linear Inverse Problems," *IEEE Transactions on Signal Processing*, **62**, 5, March 2014, pp. 1135-1146.
16. R. Piestun and D. A. B. Miller, "Electromagnetic Degrees of Freedom of an Optical System," *Journal of the Optical Society of America A*, *A*, **17**, 5, May 2000, pp. 892-902.
17. A. Capozzoli, C. Curcio, G. D'Elia, A. Liseno, and P. Vinetti, "FFT & Aperiodic Arrays With Phase-Only Control and Constraints due to Super-Directivity, Mutual Coupling and Overall Size," 30th ESA Antenna Workshop on Antennas for Earth Observation, Science, Telecommunication and Navigation Space Missions, Noordwijk, The Netherlands, May 27–30, 2008, pp. 213-216.
18. A. Capozzoli, C. Curcio, G. D'Elia, A. Liseno, and P. Vinetti, "FFT & Equivalently Tapered Aperiodic Arrays," Proceedings of the XXIX URSI General Assembly, Chicago, IL, USA, August 7–16, 2008, pp. 1-4.
19. S. C. Hawkins, "Algorithm 1009: MieSolver—An Object-Oriented Mie Series Software for Wave Scattering by Cylinders," *ACM Transactions on Mathematical Software*, **46**, 2, May 2020, p. 19.
20. T. Henriksson, N. Joachimowicz, C. Conessa, and J.-C. Bolomey, "Quantitative Microwave Imaging for Breast Cancer Detection Using a Planar 2.45 GHz System," *IEEE Transactions on Instrumentation and Measurement*, **59**, 10, October 2010, pp. 2691-2699.
21. D. S. Shumakov, A. S. Beaverstone, J. J. McCombe, and N. K. Nikolova, "Quadrupole Illumination for Improving the Signal to Noise Ratio in Microwave Imaging," 2016 10th European Conference on Antennas and Propagation, Davos, Switzerland, April 10–15, 2016, pp. 1-4.
22. A. J. Devaney and M. Dennison, "Inverse Scattering in Inhomogeneous Background Media," *Inverse Problems*, **19**, 4, June 2003, pp. 855-870.